Crystal preferred orientation of olivine in mantle xenoliths from Catalonia (NE Spain)

Orientación cristalina preferente del olivino en xenolitos mantélicos de Cataluña (NE de España)

M. Fernández-Roig[1], G. Galán[1] and E. Mariani[2]

[1] Departament de Geologia, Facultat de Ciències,

Universitat Autònoma de Barcelona, Avda. dels Til·lers s/n, 08193 Bellaterra, Barcelona, Spain
(e-mail: merce_roig@hotmail.com, gumer.galan@uab.cat)
[2] School of Environmental Sciences, University of Liverpool, 4 Brownlow Street, L60 3GP Liverpool, UK
(e-mail: mariani@liverpool.ac.uk)

Abstract: Mantle xenoliths in Neogene-Quaternary alkaline volcanic rocks from the Catalan Volcanic Zone indicate that «anhydrous» spinel lherzolites, harzburgites and much subordinate olivine websterites form the lithospheric mantle of NE Iberian Peninsula. Olivine crystal preferred orientation, determined by indexation of electron-backscattered diffraction patterns, provides three types of deformation fabric: a dominant [010]-fiber type in peridotites and websterites equilibrated at high temperature, and subordinate orthorhombic and [100]-fiber types, which appear mostly in porphyroclastic and equigranular lherzolites equilibrated at lower temperature.

Keywords: Lithospheric mantle, lherzolites, harzburgites, websterites, olivine, deformation fabric.

Resumen: Los xenolitos mantélicos en lavas alcalinas neógeno-cuaternarias de la Zona Volcánica de Cataluña indican que lherzolitas y harzburgitas «anhidras» y con espinela son las rocas predominantes en el manto litosférico del NE de la Península Ibérica, con presencia también subordinada de websteritas olivínicas. Las orientaciones cristalográficas preferentes del olivino, determinadas por indexación de los espectros de difracción de electrones retrodispersados, muestran tres tipos de fábrica de deformación: una dominante, tipo axial [010], en peridotitas y websteritas equilibradas a alta temperatura, y otras subordinadas, de tipo ortorrómbico y axial [100], que aparecen en lherzolitas porfidoclásticas y equigranulares equilibradas a menor temperatura.

Palabras clave: Manto litosférico, lherzolitas, harzburgitas, websterita, olivino, fábricas de deformación.

Mantle xenoliths enclosed in volcanic rocks along with orogenic peridotitic massifs provide unique opportunity to study the evolution of the lithospheric mantle. These xenoliths in Neogene-Quaternary alkaline basaltic rocks from the Catalan Volcanic Zone (CVZ), in NE Spain, have been previously studied in attempts to determine the composition and geochemical evolution of the subcontinental lithospheric mantle (SCLM) in this area (Bianchini *et al.*, 2007; Galán *et al.*, 2008; 2011; Galán and Oliveras, 2014). However, the deformation history of this mantle is less known. The host lavas belong to the within-plate volcanism related to the European Cenozoic Rift System (ECRIS) which lies along the Mediterranean coast.

Experimental studies demonstrate that plastic deformation related to mantle flow processes at different scales causes strong crystal preferred orientation (CPO) of olivine (Karato *et al.*, 2008 and references therein). In addition, numerical modelling shows that different deformation regimes lead to varying olivine CPO (Tommasi *et al.*, 1999). Variables include temperature (T), pressure (P) (Couvy *et al.*, 2004; Jung *et al.*, 2006; Ohuchi *et al.*, 2011), stress and H_2O concentration (Jung and Karato, 2001; Jung *et al.*, 2006; Katayama *et al.*, 2004; Katayama and Karato, 2006). CPO can also be affected by factors such as partial melting and melt percolation (Vauchez and Garrido, 2001; Holtzman *et al.*, 2003; Rampone *et al.*, 2010; Le Roux *et al.*, 2008).

Anhydrous spinel lherzolites and harzburgites are the lithologies most frequently found in mantle xenoliths from lavas of the CVZ, but much subordinate websterites are also found (Bianchini *et al.*, 2007; Galán *et al.*, 2008). The objective of this study is to characterize the olivine CPO of these xenoliths by indexation of electron-backscattered diffraction (EBSD) patterns in order to assess the deformation history of the SCLM they were extracted from.

Geological Setting

The CVZ is part of the Neogene-Quaternary volcanism of the Iberian Peninsula (Ancochea, 2004) (Fig. 1A), which in this zone was the result

of late-Alpine extensional fractures that extended the ECRIS along the Mediterranean coast (Martí, 2004 and references therein), from 35 to 0 Ma. This rifting produced extensional basins in the western Mediterranean offshore (viz., the Valencia Trough, the Gulf of Lion, the Liguro-Provençal basin) and in the Catalan margin onshore (Roca and Desegaulx, 1992).

Before the ECRIS formation, the lithosphere of this area was mainly deformed by the Hercynian orogenesis and, to a lesser degree, by the Alpine orogenesis, which led to the formation of the Catalan Coastal Ranges. Lithosphere extensive episodes with intrusion of basic magmas in between the two orogens took place during the Permian (Martínez-Poza *et al.*, 2014), when calc-alkaline to alkaline lamprophyres were intruded (Losantos *et al.*, 2000; Enrique, 2009, Ubide *et al.*, 2010), and during the Cretaceous, with intrusion of alkaline lamprophyres (Solé *et al.*, 2003; Ubide *et al.*, 2012; Esteve *et al.*, 2014).

The CVZ is divided into three subzones (Fig. 1B): L'Empordà, La Selva and La Garrotxa, which are Neogene-Quaternary basins, mainly limited by normal NW-SE faults related to neotectonic activity (11 to 0 Ma) (Lewis *et al.*, 2000). The xenoliths were found in alkaline basaltic rocks forming necks, lava flows, and pyroclasts from three volcanoes: Sant Corneli, in La Selva subzone, and Canet d'Adri and La Banya del Boc, in La Garrotxa subzone (Fig. 1B).

Protogranular is the dominant microstructure in all peridotites and pyroxenites, but lherzolite microstructures grade from protogranular to porphyroclastic and equigranular varieties. Thermobarometric estimates, using the two-pyroxene thermometer of Brey and Köhler (1990), provide higher equilibrium temperature (T) for harzburgites (1062 ± 29 ºC) and websterites (up to 1257 ºC) than for lherzolites (972 ± 89 ºC) (Galán *et al.*, 2011). More recently, Fernández-Roig and Galán (2015) found that equilibrium T in lherzolites decreases from those with protogranular microstructure (1082-950 ºC) towards porphyroclastic (959-867 ºC) and equigranular lherzolites (995-829 ºC), and that estimates using integrated compositions of clinopyroxene and/or
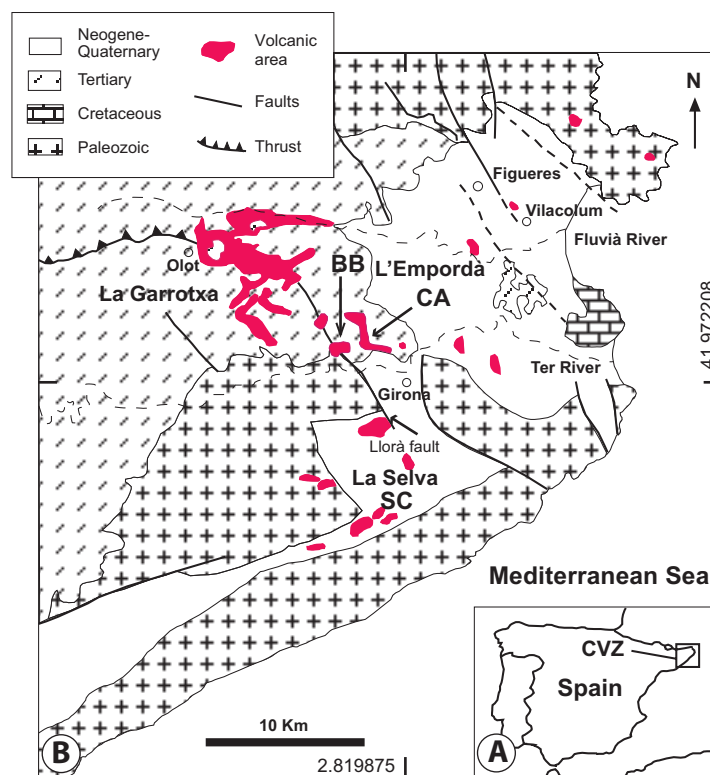
Figure 1. A) Geological location of the Catalan Volcanic Zone (CVZ) in NE Spain. B) Situation of La Banya del Boc (BB), Canet d'Adri (CA) and Sant Corneli (SC) volcanoes. Map modified after Solé Sabaris (1962) and Tournon (1968). Geographic ETRS89 coordinates are indicated.

clinopyroxene porphyroclasts and mutual exsolved lamellae (1125-955 ºC) are higher and comparable to those registered by protogranular lherzolites and harzburgites. Decreasing T from protogranular towards porphyroclastic and equigranular peridotites was also found in similar xenoliths from the Carpathian-Panonian region (Szabó *et al.*, 2004). On the other hand, lherzolites record a wider range of pressure (P) (1.88 ± 0.60 GPa) than harzburgites (1.02 ± 0.19 GPa) (Galán *et al.*, 2011; Fernández-Roig and Galán, 2015); estimates from the clinopyroxene-olivine thermobarometer of Köhler and Brey (1990). Decreasing P from protogranular to porphyroclastic and equigranular lherzolites is consistent with decreasing jadeite component of their clinopyroxene (Fernández-Roig and Galán, 2015). These xenoliths are classified as off-craton type and according to Galán and Oliveras (2014), lherzolites and harzburgites are products of melt depletion and subsequent metasomatism. However, they do not excluded that some lherzolites, with clinopyroxene displaying depletion in light

rare earth elements (LREE) and Depleted MORB Mantle (DMM) isotopic compositions, could have been formed by refertilization of refractory, but isotopically enriched harzburgites, via percolation and reaction with N-MORB type basalts. Galán and Oliveras (2014) also found that harzburgites register multi-stage metasomatism. An earlier episode was caused by subduction-related hydrous fluids or melts and the second metasomatism was mainly cryptic and related to the percolation of alkaline silicate melts and carbonatite derivatives. This latter metasomatism also affected a few lherzolites. Websterites are interpreted as cumulates from the mafic alkaline silicate melts that caused the second metasomatism (Galán *et al.*, 2008).

Methods

The mineral mode (% volume) of the studied rocks was determined using the petrographic microscope with a precision stepping stage and an automatic

Rock type	Olivine	Orthopyroxene	Clinopyroxene	Spinel
PG Lhz	50-65	28-37	7-14	<5
PG-PC Lhz	47-63	23-40	9-11	<5
PC Lhz	46-57	27-33	8-16	<8
EG Lhz	42-63	26-37	10-17	<5
PG Hz	70-73	23-27	1-4	<2
PG Wb	19	27	54	0

Table 1. Variation of mineral mode (wt% volume) of different lherzolites (Lhz), harzburgites (Hz) and the websterite (wb).

PG: protogranular; PC: porphyroclastic; EG: equigranular

James Swift point counter. A synthesis of the mineral mode is included in Table 1. Thin sections were cut in random orientation since the foliation and lineation could not be determined clearly in most hand speciments.

Thin sections were prepared for quantitative crystallographyc analyses, using electron backscatter diffration (EBSD) (Ben Ismaïl and Mainprice, 1998; Prior *et al.*, 2009) by performing chemo-mechanical polishing with a 0.05 μm colloidal silica solution, and then coating with 4nm thick carbon layer to avoid charging issues in the scanning electron microscope (SEM). EBSD was carried out in the EBSD-SEM Laboratory in the School of Environmental Sciences at the University of Liverpool, using two different SEMs: a XL30 tungsten filament SEM and a CamScan X500 CrystalProbe field emission gun (FEG) SEM, both equipped with EBSD-EDS systems from Oxford HKL Technology. Automatic orientation mapping was carried out over the entire thin section area (~ 30 mm × 25 mm) of three samples (SC.11.16, BB.08.20, BB.08.101), and over an area of ~ 15 mm × 20 mm for the remaining thin sections, with sampling steps ranging from 30 to 50 μm and based on the sample's grain size. Accelerating voltage and working distance were 20 kV and 25 mm respectively. The Channel 5 software was used for automated indexing of all minerals present and for processing EBSD datasets. Indexation rates in the raw maps were ~ 65%. Mean angular deviation (MAD), which shows the match between lattice planes in a calculated orientation and measured lattice planes in EBSD patterns, was commonly < 1 ° (mainly ≈ 0.6 °). Non-indexed areas resulted from fractures, alteration, basalt zones, grain boundaries and polishing defects. Post-acquisition data processing allowed us to improve the indexation rate by using grey-scale values of band contrast images to constrain areas where non-indexed pixels could be filled with the average orientation of neighbouring pixels. During this process, isolated single pixels representing points misoriented ≥ 10 ° from the average orientation of surrounding pixels were removed first (i.e., wild spikes). Then, empty pixels were replaced with the most common neighbouring orientation, if they had up eight identical neighbours. This process was repeated using sequentially seven, six, five and four identical neighbours. At each step great care was taken by using both band contrast images and micrographs to ensure that no artifacts were introduced into datasets. This method minimizes the over-counting of individual grains when extracting one orientation point per grain for the construction of pole figures.

Olivine CPO data are displayed in pole figures, presented as lower hemisphere stereographic projections, using the PFctf programme by Mainprice (ftp://www.gm.univ-montp2.fr/mainprice//CareWare_Unicef_Programs/). To avoid over-representation of coarse grains, pole figures were plotted by considering one point per grain. To facilitate comparison of CPO between different samples whose lineation and foliation could not be identified clearly in hand specimen, the data were rotated to a standard position, using the ROTctf programme by Mainprice, with the maximum concentration of olivine [100] and [010] axes parallel to the E–W and the N–S direction, respectively. This orientation would correspond to that expected in a sample with a horizontal E–W lineation (structural X direction) and a vertical foliation plane (normal to the structural Z direction), if olivine had been deformed by dislocation creep with dominant activation of the high-temperature, low-stress (010)[100] slip system (Ben Ismaïl and Mainprice, 1998). Therefore, when we refer to "lineation" and "folitation" from now on, it must be

understood they are apparent. Finally, the rotation axes that accommodate low-angle misorientations (2-15 °) are analysed in EBSD maps of a selected sample and displayed on inverse pole figures.

The fabric strength (Bunge, 1982) was estimated from the dimensionless number J-index= $\int f(g)^2$ dg (Ben Ismaïl and Mainprice, 1998), where f(g) is the density in the orientation distribution function at orientation g, and dg = $d\phi 1 d\Phi d\phi 2 sin\Phi/8\pi^2$, where $\phi 1$, Φ and $\phi 2$ are the Euler angles that define the rotations which allow for comparison between the crystallographic and external reference frames (Bunge, 1982). The J-indices for all samples were calculated from the mean orientation of each grain using the SuperJctf software by Mainprice: ftp://www.gm.univmontp2.fr/mainprice//CareWare_Unicef_Programs/, using a 10 ° Gaussian half-width, 1 ° cells, and truncation of the orientation distribution function at 22 °.

Further analysis of the mineral CPO symmetries was performed using the point (P), girdle (G) and random (R) fabric-type indices for olivine [100], [010] and [001] axes. These indices were calculated from the three eigenvalues ($\lambda 1$, $\lambda 2$, $\lambda 3$) of the normalized orientation matrix (Woodcock and Naylor, 1983; Humbert *et al.*, 1996) for each principal crystallographic axis as: P = $\lambda 1–\lambda 3$, G = 2($\lambda 2–\lambda 3$) and R = 3 $\lambda 3$ (Vollmer, 1990) and can be combined for a more throughout analysis of CPO symmetry. The BA-index= 0.5 * (2.0 – (P010 / (G010 + P010)) – (G100 / (G100 + P100))) (Mainprice et al, 2015) was used for classifying olivine deformation fabric or symmetry. As this numerical classification does not require knowledge of the orientation of the specimen reference frame in absolute terms, it is convenient for analysing mantle xenoliths.

Petrography of xenoliths

Eighteen xenoliths were selected for indexing the CPO. The selection was based on size, with those of ca., 2×4 cm or larger being regarded as the most suitable. The petrography and geochemistry of one of them (CA.44.05) was previously studied by Galán *et al.* (2011) and Galán and Oliveras (2014),

whereas only previous mineralogical data and T and P estimates were published for the remaining samples (Fernández-Roig and Galán, 2015). The selected xenoliths are representative of the main lithologies found in the SCLM beneath the CVZ (Galán *et al.*, 2008) and include thirteen spinel lherzolites, one plagioclase-spinel lherzolite, three spinel harzburgites, and one olivine websterite. All are "anhydrous" exception made of one lherzolite (BB.08.59), which has accessory amphibole forming scarce disseminated anhedral crystals (≈100 μm in size), and the single websterite, which has phlogopite in sparce subhedral crystals (500-1000 μm at their long axis).

Lherzolites represent 60% of the total xenoliths sampled so far, of which 36% are protogranular, 15% are porphyroclastic and 9% are equigranular (Fernández-Roig and Galán, 2015); microstructure terms after Mercier and Nicolas (1975). Mineral mode ranges of protogranular lherzolites (BB.08.101, BB.08.98, BB.12.01, CA.44.05) (Fig. 2A) show the highest amount of olivine and the lowest of clinopyroxene of all lherzolites, although these ranges overlap largely between lherzolites with different microstructures (Table 1). Protogranular lherzolites also present grain size ≥ 2 mm (Harte, 1977), with olivine and orthopyroxene forming the largest crystals (2-5 mm at their long axis), whereas clinopyroxene and spinel crystals are smaller (< 2 mm). Elongated and orientated olivine crystals in two of these protogranular lherzolites (BB.08.101, BB.08.98) also define tabular microstructural varieties. All crystals are anhedral with straight or slightly curved grain boundaries, occasionally at 120°, especially between olivine crystals, with more interlobate boundaries when seen next to other minerals, e.g., bordering orthopyroxene crystals. Orthopyroxene can include small rounded olivine crystals. Spinel also forms interstitial brownish-green or green crystals (up to 1700 μm in size) with frequent embayed grain boundaries. These crystals can also include round shaped olivine and orthopyroxene crystals and be orientated. Other forms of spinel are lamellae within both pyroxenes. Clinopyroxene crystals (0.5 < grain size < 2 mm) show either straight or gently curved grain boundaries. Olivine (and more rarely orthopyroxene) show sporadic evidence of deformation and recovery, such
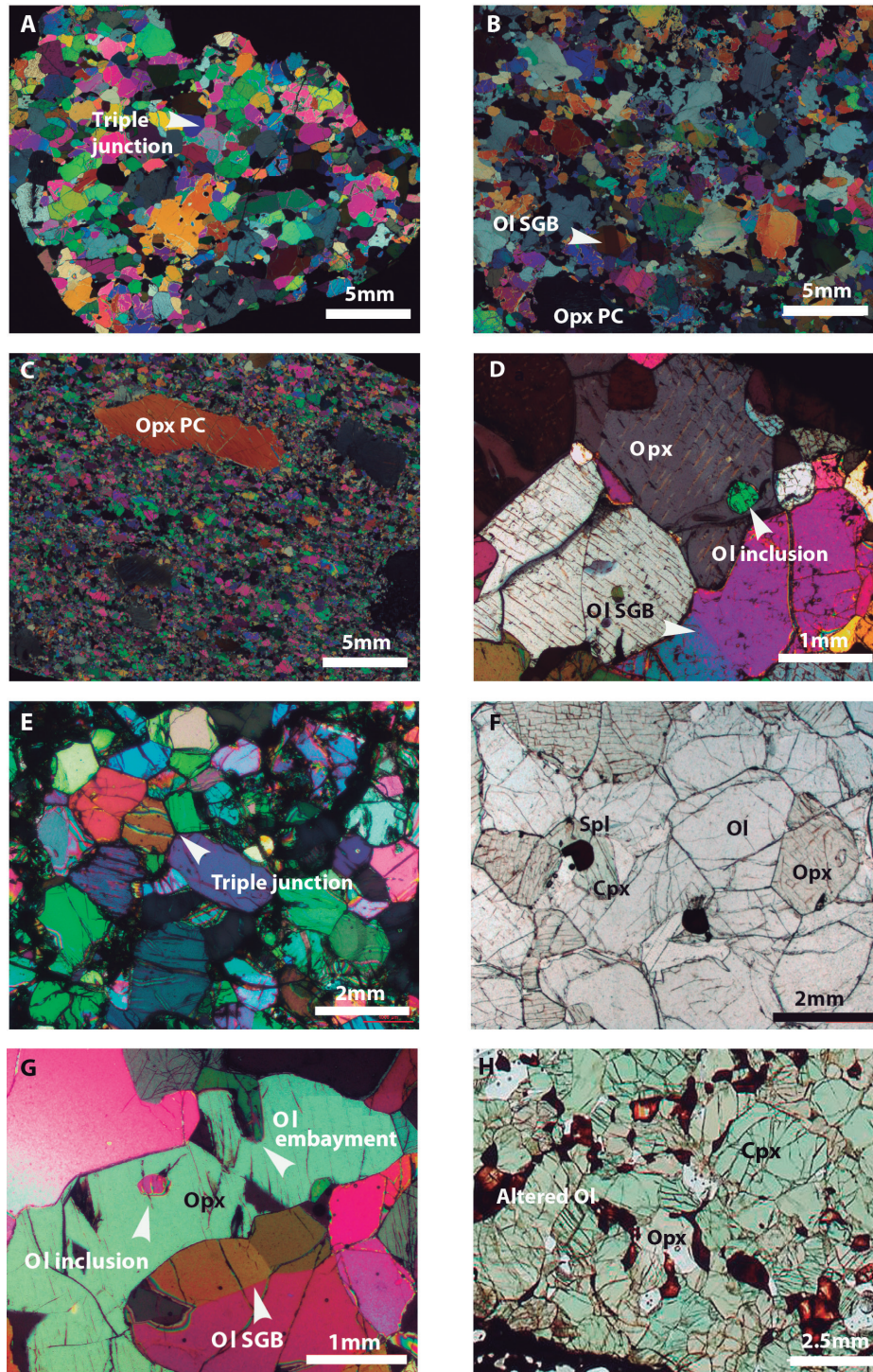
Figure 2. Microstructures of the mantle xenoliths. A) Protogranular lherzolite (BB.08.98); note the triple junctions between olivine grain boundaries. B) Lherzolite (BB.08.59) with protogranular-porphyroclastic transitional microstructure, orthopyroxene porphyroclasts (PC) and subgrains (SGB) in olivine crystals. C) Elongated orthopyroxene porphyroclasts, in a finer-grained tabular matrix (lherzolite SC.11.16). D) Subgrains in olivine and olivine inclusion in orthopyroxene of lherzolite BB.08.98. E) Equigranular lherzolite (SC.11.54) with grain boundaries at 120º. F) Interstitial anhedral spinel crystals in protogranular harzburgite BB.08.20. G) Olivine embayment and olivine inclusion in an orthopyroxene crystal of harzburgite CA.12.02. H) Protogranular websterite with olivine crystals partially altered to iddingsite (BB.12.17).

as undulose extinction, deformed exsolved lamellae, deformation bands and widely spaced subgrain boundaries.

Two lherzolites with transitional protogranular-porphyroclastic microstructure (BB.08.59, BB.12.13) mainly differ by including alternating protogranular and finer grained (0.3 < grain size < 2 mm) areas without any specific arrangement (Fig. 2B). In the former, there is more evidence of intracrystalline deformation in olivine and orthopyroxene crystals and more frequent exsolved clinopyroxene lamellae in orthopyroxene than in the protogranular lherzolites. In the finer-grained areas, recrystallized strain-free neocrysts, or with rare subgrains, and frequent grain boundaries at 120° dominate. Spinel appears either as isolated interstitial crystals (up to 3 mm at their long axis) or more rarely as amoeboid crystals intergrown with orthopyroxene, as «clusters».

Porphyroclastic lherzolites (SC.11.16, SC.11.49, SC.11.52, BB.08.80, CA.12.03) have mineral mode range overlapping that of protogranular lherzolites (Table 1). SC.11.49 stands out for having plagioclase along with olivine, orthopyroxene and chromite forming coronae around spinel crystals. These rocks include mainly orthopyroxene porphyroclasts (3-11 mm in size) and less frequently olivine, clinopyroxene and spinel porphyroclasts, in a much finer matrix (0.2 < grain size < 1 mm) made up of slightly deformed or strain-free neocrysts, or with sporadic subgrains, of the same minerals (Fig. 2C). Orthopyroxene porphyroclasts display evident features of intracrystaline deformation, such as frequent bent clinopyroxene and spinel lamellae at the core, undulose extinction, kinks bands and more closely spaced subgrain boundaries than in the protogranular lherzolites. They also display embayed grain boundaries against strain-free olivine neocrysts that can be seen as rare inclusions (Fig. 2D). Spinel porphyroclasts are amoeboid crystals intergrown mainly with orthopyroxene. They can be very stretched and along with orthopyroxene porphyroclasts define a clear orientation (e.g., in SC.11.16). Spinel neocrysts are smaller (≈ 60 μm), rounded and interstitial between silicates. Clinopyroxene is mainly as isolated and elongated clustered neocrysts. Spinel lamellae are frequent in both clinopyroxene neocrysts and rare porphyroclasts.

Most equigranular lherzolites (BB.08.38, BB.08.57, SC.11.54) are also tabular because elongated olivine neocrysts are orientated. Their mineral mode overlaps largely that of the other lherzolites, but they show the highest amount of clinopyroxene. The rare porphyroclasts (< 5 wt%) are mainly of orthopyroxene (grain size up to 5 mm), in a finer grained matrix, where spinel is usually as interstitial rounded brown, rarely green, crystals or elongated crystals with lobate grain boundaries. Average grain size is usually < 1 mm in most samples. Grain boundaries are generally straight or slightly curved among neocrysts, with frequent tripe junctions (Fig. 2E). Intracrystalline deformation or recovery features are absent or are very sporadic.

Protogranular harzburgites (BB.08.20, CA.12.02, BB.12.04) represent 36% of the total mantle xenoliths. The mineral mode range is displayed in Table 1. Microstructure features are similar to those of protogranular lherzolites but they differ in the following aspects: (i) olivine and orthopyroxene crystals are coarser grained (2-6 mm); (ii) spinel crystals (100 < grain size < 700 μm) are generally darker brown, anhedral and interstitial, and more rarely amoeboid (Fig. 2F); and (iii), intracrystalline deformation or recovery features (subgrains) are sparser than in lherzolites. Olivine embayment in orthopyroxene, with both minerals presenting mutual inclusions, are common in sample CA.12.02 (Fig. 2G). Moreover, harzburgite BB.12.04 stands out by showing tabular protogranular microstructure.

The websterite BB.12.17 is also protogranular (Fig. 2H), with average grain size of 2-3 mm, straight or gently curved grain boundaries and few deformation effects: only olivine crystals, which are partially altered to iddingsite, display undulose extinction and deformation bands.

Olivine crystal preferred orientations

All the harzburgites, nine of the lherzolites and the websterite show the same olivine deformation fabric: [010]-fiber or AG type (Ben Ismaïl and Mainprice, 1998; Mainprice, 2007), characterized by point concentration of [010] parallel to Z and normal girdles of [100] and [001] axes within the structural

X-Y plane ("foliation") (Fig. 3). The main slip system is (010)[100]. BA indices for these samples range from 0.09 to 0.39 (Fig. 3). The higher main density (MD) corresponds mostly to the [010] axis and [100] axis shows higher MD than [001] except in two samples (CA.44.05, BB.12.17), where it is the reverse. Four other lherzolites display orthorhombic (Tommasi *et al.*, 1999) (A-type after Jung and Karato, 2001) deformation fabric characterized by orthogonal point concentrations of the three olivine axes. The higher MD corresponds to [010] axis in two samples and to [100] and [001] axes in the other two cases (BB.08.57 and CA.12.03, respectively). The dominant slip system is also (010)[100]. The BA indices range from 0.42 to 0.48. Finally, only one lherzolite shows [100]-fiber (D-type after Karato *et al.*, 2008) or deformation fabric defined by strong point concentration of [100], and girdles of [010] and [001] axes parallel to each other and normal to [100] (Fig. 3). In this case, [100] axis shows the highest MD, the dominant slip system is {0kl}[100] and the BA index is 0.78. In spite of this numerical classification based on the BA index, there are transient fabrics between the three types in some lherzolites (Fig. 3). For example, the fabric of CA.44.05 can be considered transitional AG-A type because [100] and [001] axes tend to point concentrations. Other cases are transitional AG-D type (BB.08.38, SC.11.52, SC.11.54) since [001] axis tends to be normal to the "foliation" plane instead of being within it. Finally, the fabric of lherzolite BB.08.57 can be considered transitional A-D type for the same reason: [001] axis tends to be normal to the "foliation" plane. It should be noted that [100] and/or [001] axes are bimodal in two lherzolites with AG-D type fabric (BB.08.38, SC.11.52). For these examples, one [001] maximum is aligned with [100] axis and the other with [010] (Fig. 3). Finally, the fabric strength (i.e., J index) is variable. The highest values (10.12-5.43) correspond to harzburgites and the lherzolites which have well defined AG-type fabric. The websterite also follows this pattern. J indices for the other lherzolites range from 4.69 (A-type fabric) to 1.91 (transitional AG-D-type fabric) (Fig. 3).

J indices vs. BA indices display scatter, although negative correlation is observed overall (Fig. 4A). No clear relationships exist between BA indices and the microstructure types (not shown), although all BA values > 0.40 correspond to porphyroclastic lherzolites. However, a better relationship is displayed between J indices and the microstructure types: J indices clearly decrease from protogranular harzburgites and lherzolites towards porphyroclastic and equigranular lherzolites (Fig. 4B), which overlap both. Therefore, it is inferred that a general positive correlation exists between the fabric strength and the equilibrium T since both variables decrease from protogranular harzburgites, lherzolites and the websterite towards porphyroclastic and equigranular lherzolites (Fernández-Roig *et al.*, 2015a, b). Finally, J indices are positively and negatively correlated with olivine (Fig. 4C) and clinopyroxene mode (not represented), respectively, in protogranular (-porphyroclastic) harzburgites and lherzolites. Nevertheless, porphyroclastic and equigranular lherzolites do not follow these trends (Fig. 4C).

Misorientations

Deformation by dislocation creep causes not only the existence of characteristic CPO but also of distinct misorientations, i.e., changes in crystallographic orientation between two points. Misorientations can occur within grains or across low-angle grain boundaries (i.e., subgrains). Since rotation axes of subgrains depend on the dislocations which form the boundaries (edge dislocations) (Frank, 1950; Amelinckx and Dekeyser; 1959), they can be used to infer the active slip systems during deformation (Lloyd *et al.*, 1991). To this end the orientation of the trace of subgrain boundaries of olivine crystals (Fig. 5) and inverse pole figures (IPFs) of the rotation axes (< 15 °) were considered (Fig. 3). For instance, the olivine crystals from the protogranular harzburgite BB.08.20 **(**Figs. 5a-b) have mainly subgrain boundaries with a trace subnormal to the [100] axis. This implies that the subgrain walls are mainly tilt boundaries composed of dislocations slipping in the [100] direction. Accordingly, the corresponding IPF (Fig. 5c) illustrates that the rotation axes are distributed between [001] and [010] axes, which indicates that the subgrain walls were mainly formed by dislocations of the {0kl}[100] slip systems or "pencil glide". Therefore, if deformation was mainly accommodated by "pencil glide" dislocations, the
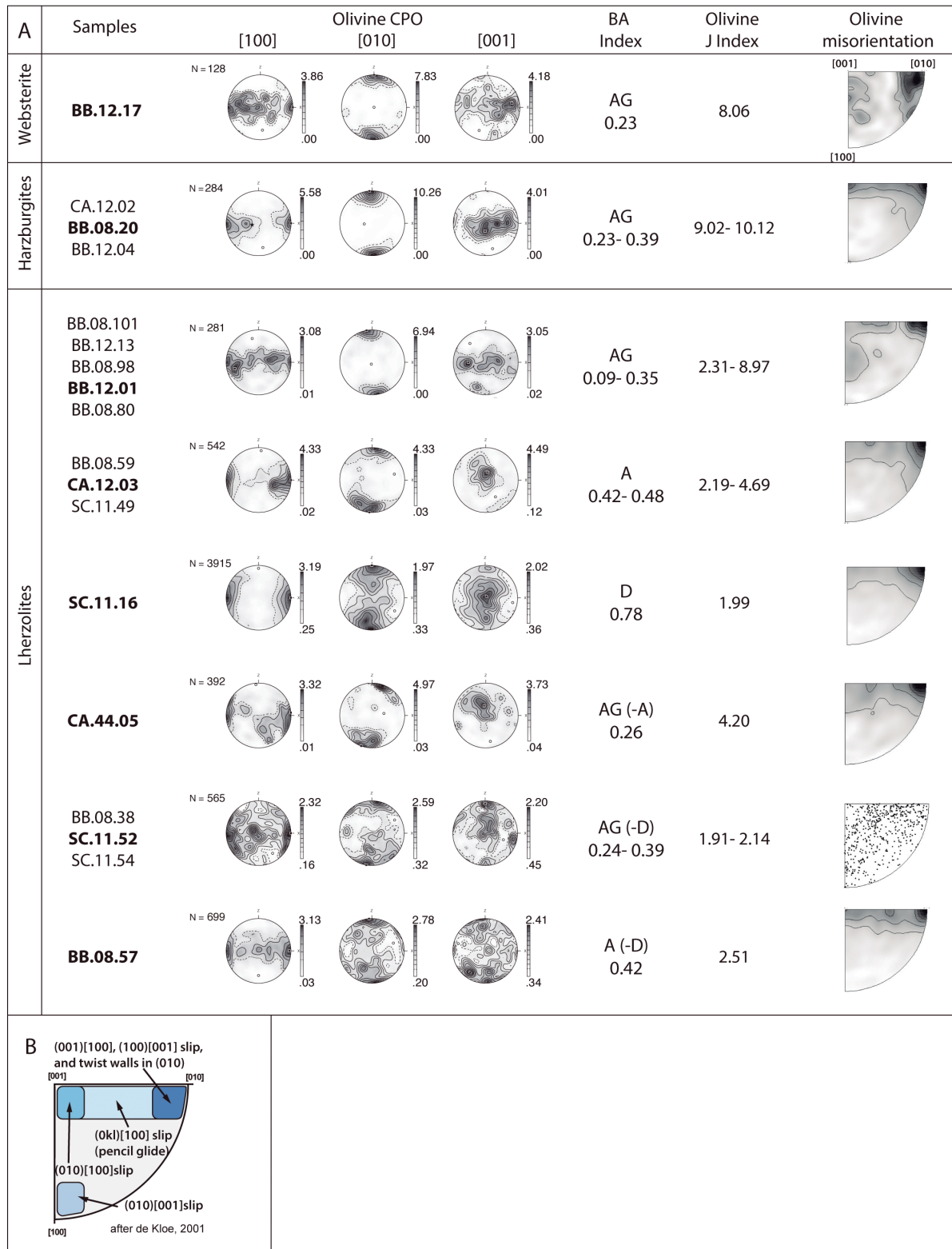
Figure 3. Representative stereograms for olivine CPOs rotated to match olivine [100] and [010] axes with structural X and Z directions, respectively. Values of J index (Ben Ismaïl and Mainprice, 1998) and the deformation fabric types of olivine according to values of BA index (Mainprice *et al.*, 2015). Represented sample is in bold and similar ones are included. Inverse pole figures for olivine rotation axes accommodating misorientations of less than 15º are also shown (contours at 1.0 multiples of a uniform distribution intervals).
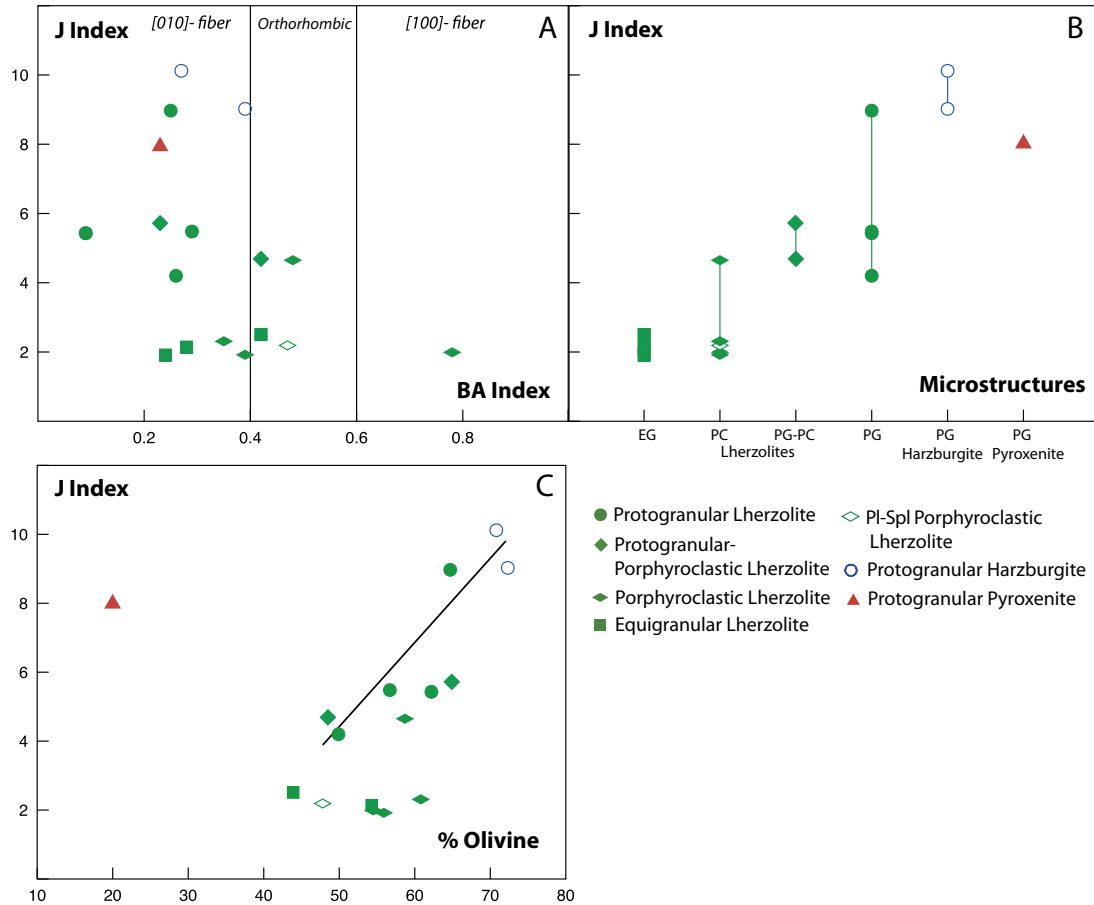
Figure 4. A) J index vs. BA index. B) Relationships between J index and microstructures. C) J index vs. olivine mode. There is a positive correlation between protogranular (PG) (-porphyroclastic) peridotites, but porphyroclastic and equigranular lherzolites display scatter.

assumption that olivine [100] maximums are parallel to the lineation would be corroborated. In the other xenoliths, the activation of the {0kl}[100] slip systems is consistent with the distribution of the rotation axes between [001] and [010] axes in the IPFs (Fig. 3). In most samples, we observe either similar densities for the distribution of [001] and [010] rotation axes or [010] maximums (61% of the total samples). This suggests the predominance of the (001)[100] slip system over the (010)[100] in more than half of the xenoliths, contradicting the dominant slip system deduced from the AG- and A-type olivine deformation fabrics. This partial disagreement has been observed in other peridotites (Soustelle *et al.*, 2010; Falus *et al.*, 2011; Kaczmarek and Tommasi, 2011; Zaffarana *et al.*, 2014), which leads to the conclusion that dislocations in subgrain boundaries

may not be completely representative of the slip system activity. Alternatively, the predominance of the olivine [010] rotation axes could imply the activation of the (100)[001] slip system (de Kloe, 2001) (Fig. 3).

Deviatoric stress estimates

Recrystallized, strain-free finer-grained (0.2 < grain size < 1 mm) crystals (neocrystals) in lherzolites with protogranular-porphyroclastic, porphyroclastic and equigranular microstructures have been used to estimate the stress during their deformation. The relationship between the two variables is:

$$D_g = A\sigma^{-n} \tag{1},$$
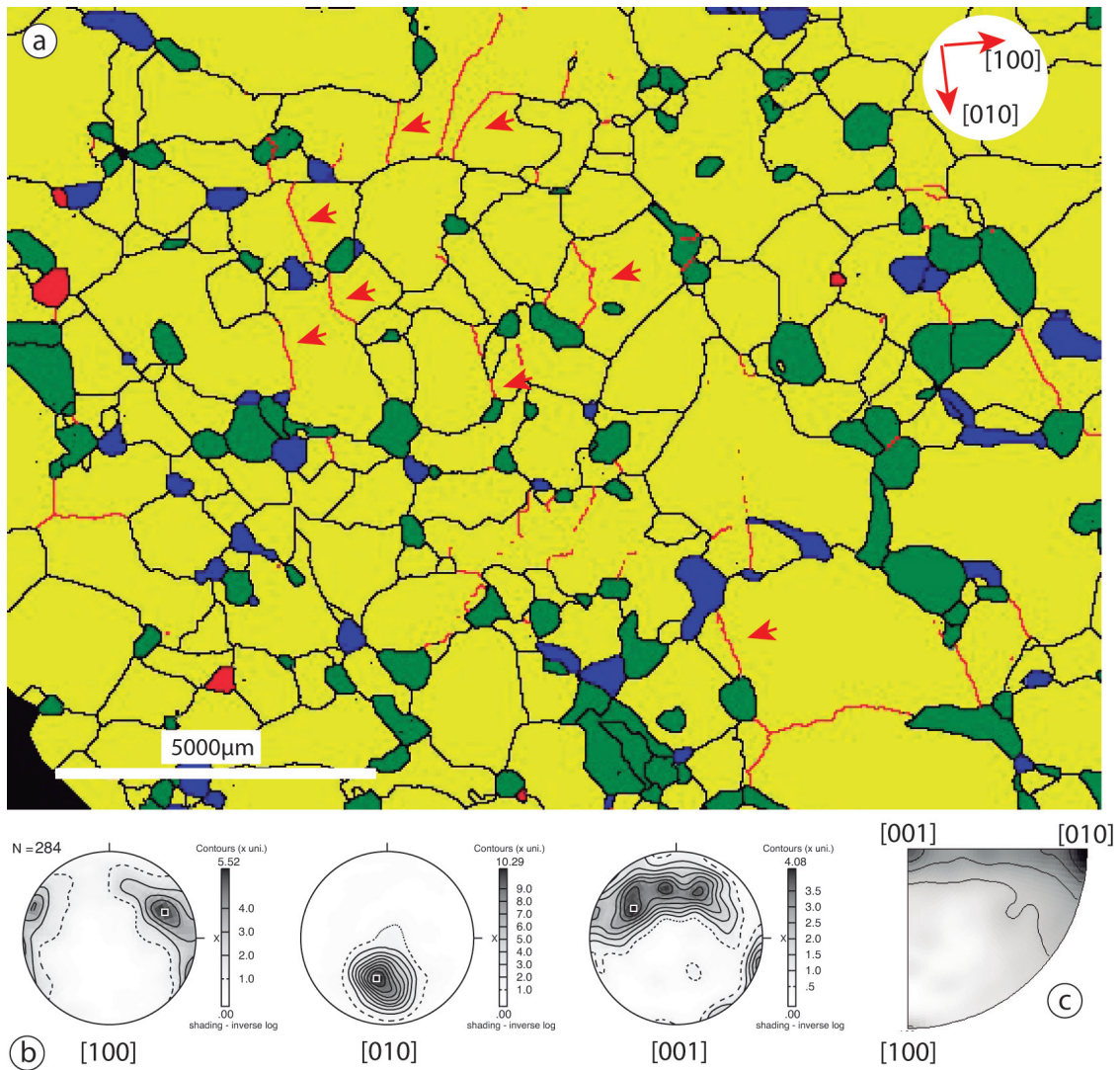
Figure 5. a) Processed EBSD map of the protogranular harzburgite BB.08.20, with different colours standing for different minerals: yellow-olivine, blue-orthopyroxene, green-clinopyroxene, red-spinel. Traces of subgrain boundaries in olivine crystals are in thin red lines. The most frequent subgrain boundaries are highlighted with red arrows and are subnormal to olivine [100] axis, suggesting the existence of dislocations slipping in [100]. b) Stereograms for the olivine CPO of the whole sample in the original position (not rotated). c) Inverse pole figure for the rotation axes of the olivine crystals accommodating misorientations of less than 15º.

where D_g is the recrystallized grain size, σ is the differential stress, and A and n are empirical constants obtained by fitting experimental data. In this study, we used the calibrations of Karato *et al.* (1980) (A=8300; n=1.18) and of Van der Wal *et al.* (1993) (A=15000; n=1.33). The grain size was measured using the EBSD crystallographic orientation maps (not shown). Average grain size ranges from 960 μm in the protogranular-porphyroclastic lherzolite BB.12.13 to 360 μm in the porphyroclastic sample SC.11.16, which gives stress of 6.1-14.1 MPa

(Karato *et al.*, 1980) or 8.0-16.7 MPa (Van der Wal *et al.*, 1993).

Discussion

The origin of olivine CPO

Previous results indicate that the dominant deformation fabric in the studied xenoliths is AG-type (Fig. 3), which also shows the highest fabric

strength. This indicates deformation by dislocation creep at high T, dry conditions and low stress (Carter and Avé Lallemant, 1970; Tommasi *et al.*, 1999). AG-type fabric was once thought to be less common than the A- and D-types in mantle rocks (Mainprice, 2007) but it has since been found in samples of both orogenic peridotitic massifs (Vauchez and Garrido, 2001; Tommasi *et al.*, 2006; Le Roux *et al.*, 2008; Kaczmareck and Tommasi, 2011; Higgie and Tommasi, 2014) and mantle xenoliths: cratonic (Ben Ismaïl *et al.*, 2001; Vauchez et al., 2005, 2012), off-craton (Tommasi *et al.*, 2008; Hidas *et al.*, 2007; Kovács *et al.*, 2012) and in oceanic within-plate context (Vonlanthen *et al.*, 2006; Bascou *et al.*, 2008). In some of these examples, AG-type deformation fabric is dominant, as in the Ronda (Betic orogenic belt, S Spain) and Lanzo massifs (western Alps; Italy) (Vauchez and Garrido, 2001; Soustelle *et al.*, 2009; Higgie and Tommasi, 2014), the mantle xenoliths of Tok (SE Siberia) (Tommasi *et al.*, 2008) and of the Kerguelen islands (Indian ocean) (Bascou *et al.*, 2008). However the AG-type fabric may be subordinate to other types, as in the nearby peridotitic massif of Lherz (Eastern Pyrenees, France), where D-type fabric is dominant (Le Roux *et al.*, 2008).

Hypotheses for the origin of AG-type fabric are: (1) deformation by axial shortening, transpression or simple shear (Tommasi *et al.*, 1999; Vauchez *et al.*, 2000; Kovács *et al.*, 2012); (2) melt assisted shear deformation at high T and P (Holtzman *et al.*, 2003; Le Roux *et al.*, 2008; Higgie and Tommasi, 2014); (3) simultaneous activation of the (010)[100] and (010)[001] slip systems under high stress and/or high water content or high P conditions (Tommasi *et al.*, 2000; Mainprice *et al.*, 2005; Vauchez *et al.*, 2005; Hidas *et al.*, 2007; Bascou *et al.*, 2011; Jung *et al.*, 2014); and (4), static recrystallization (annealing) (Tommasi *et al.*, 2008; Zaffarana *et al.*, 2014). Data of this study are consistent with hypothesis (1). Hypothesis (2) posits that melt assisted shear deformation, either during mantle partial melting (Vauchez and Garrido, 2001; Soustelle *et al.*, 2009) or during melt-rock reaction due to percolation of basaltic magmas (i.e., igneous refertilization of the lithospheric mantle). In a mantle partial melting process, the amount of olivine would be increased due to incongruent melting of orthopyroxene. In

melt-rock reaction processes there are at least two posssibilities: (i) orthopyroxene would be increased at clinopyroxene expense, if the percolating melt is SiO_2 oversaturated (Kelemen *et al.*, 1992); and (ii), olivine would be dissolved and pyroxenes± spinel, garnet or plagioclase be crystallized, if refertilization reactions had taken place during the basaltic percolation (Dijkstra *et al.*, 2003; Le Roux *et al.*, 2007; Bodinier *et al.*, 2008; Kaczmarek and Müntener, 2008; Johanesen and Platt, 2015). In the studied example, the positive and negative correlation of olivine (Fig. 4C) and clinopyroxene modes, respectively, with respect to J indices of xenoliths with AG-type fabric suggests that if refertilization had occurred, it would have weakened instead of strengthening this fabric. This is contradictory with hypothesis (2). Other microstructural evidence associated with refertilization processes are: interpenetrating olivine-pyroxene boundaries (Dijkstra *et al.*, 2003; Soustelle *et al.*, 2009; Higgie and Tommasi, 2014; Zaffarana *et al.*, 2014) and olivine inclusions in pyroxenes (Zaffarana *et al.*, 2014). While figure 2G shows evidence of olivine embayment and olivine inclusions in orthopyroxene, it remains the case that both textural features (see also Fig. 2D) can also be explained as left-over crystals resulting from grain boundary migration (GBM) recrystallization (Passchier and Trow, 2005) and so they are not conclusive. However, refertilization of refractory harzburgites giving rise to lherzolites, via percolation of MORB-type basaltic melts, cannot be discounted as the origin of some of the CVZ lherzolites. These show clinopyroxene with LREE depletion and DMM Sr and Nd isotopes (Galán and Oliveras, 2014), all geochemical characteristics of refertilized lherzolites from the neighbouring ultramafic Lherz massif (Le Roux *et al.*, 2007). As regards hypothesis (3), simultaneous activation of the slip systems (010)[100] and (010)[001] as the origin of AG-type fabric, does not account for the P-T equilibrium conditions of the studied rocks within the spinel lherzolite field. These P-T conditions are lower than those considered for the activation of [001] glide in experimental studies (Couvy *et al.*, 2004; Mainprice *et al.*, 2005; Jung *et al.*, 2006; Ohuchi *et al.*, 2011). This would be in agreement with the fact that the MD of olivine [100] axis is greater than that of [001] in most xenoliths with AG-type fabric. It is worth noting that the presence of H_2O could have favoured

the simultaneous activation of both slip systems at lower P (Jung *et al.*, 2014). This could explain the fact that the MD of [001] axis is greater than [100] MD in samples CA.44.05 and BB.12.17, the latter with phlogopite. However, unless H_2O were present in anhydrous minerals, this option would be unlikely since hydrous minerals are rare or absent in most xenoliths. Finally, static recrystallization or annealing (hypothesis 4) seems to be compatible with: (i) the coarse-grained microstructure characteristic of protogranular peridotites and the websterite, most of them with olivine AG-type fabric (Figs. 2A, F, H); (ii) the straight or slightly curved grain boundaries and interfacial angles at 120° among olivine crystals (Figs. 2A, F); and (iii), higher T estimates for these rocks (Fernández-Roig and Galán, 2015). Grain growth by grain boundary area reduction (GBAR) would have taken place simultaneously or subsequent to deformation mechanisms, such as subgrain rotation (SR) and GBM recrystallization. In summary, the annealing hypothesis (4) is the most credible explanation for the origin of olivine AG-type deformation fabric of the studied SCLM. However, the possibility of the olivine AG-type fabric being inherited from earlier deformation stage(s) caused by transpression or simple shear (hypothesis 1) cannot be completely ruled out since annealing does not necessarily modify previous fabric (Vauchez and Garrido, 2001). The presence of melt (hypothesis 2) could also have been a factor in deformation and/or annealing events. Thus, since olivine AG-type fabric exists in harzburgites, lherzolites and the websterite, and since the pyroxenites were interpreted as cumulates from percolating alkaline mafic silicate melts causing cryptic metasomatism in most harzburgites and a few lherzolites (Galán *et al.*, 2008), it is likely that annealing was promoted by the percolation of these metasomatic melts and derivatives.

The other olivine deformation fabrics, A-(orthorhombic) and D- ([100] fiber) types, are mainly characteristic of mainly finer-grained protogranular-porphyroclastic, porphyroclastic and equigranular lherzolites (Fig. 3), and show lower fabric strength. According to experimental data (Jung and Karato, 2001), both are developed by simple shear deformation at dry conditions, low to moderate stress (A-type), high stress (D-Type), and high T, but lower for D-type with respect to A-type. Numerical simulations of CPO by Tommasi *et al.* (1999) also indicate deformation by pure shear or plane transpression for the A-type and transtension for the D-type fabric. Considering that both types of CPO are found in samples equilibrated at lower T and P than those with AG-type fabric (Fernández-Roig and Galán, 2015) and that A- and D-types range to the AG- type (Fig. 3), we suggest that the AG-type was an earlier deformation fabric transformed into A- and D-types by changes in the deformation regime, from mainly transpressional to simple shear or transtensional. These changes happened at higher stress and lower T and P (Fernández-Roig *et al.*, 2015a, b). The same conclusion was drawn after the study of mantle xenoliths displaying similar characteristics in the southeastern Carpathians and San Quintin (Baja California) (Falus *et al.*, 2011; Palasse *et al.*, 2012 and references therein). The evolution of the olivine fabric in extensional shear zones of orogenic peridotitic massifs is also in agreement: for instance, in the northern Lanzo shear zone (Kaczmarek and Tommasi, 2011). Deformation at decreasing T and P is consistent with: (i) higher T estimates from original compositions of orthopyroxene and clinopyroxene porphyroclasts than from neocrystals; (ii) a lower jadeite component in clinopyroxene found in porphyroclastic and equigranular lherzolites (Fernández-Roig and Galán, 2015); and (iii), possible activation of the olivine slip system (100)[001] along with the dominants {0kl}[100], as deduced from misorientations (Fig. 3) (Carter and Avé Lallemant, 1970; Tommasi *et al.*, 2000 and references therein). The third option is supported by the fact that in four xenoliths, the MD of olivine [001] and [100] axes are similar or slightly higher that of [001] (e.g., CA.12.03 in Fig. 3). Deformation would have been accommodated mainly by SR and GBM recrystallization. Evidence of accommodation by grain boundary sliding has not been observed, e.g., four-grain junctions (Lee *et al.*, 2002). However, Soustelle *et al.* (2009, 2010) and Zaffarana *et al.*, (2014) suggest that decreasing J index at decreasing and increasing olivine and pyroxene mode, respectively (Fig. 4C, Table 1), as it happens in porphyroclastic and equigranular lherzolites with A- and D-type fabrics of this study, is due to syn- to post-kinematic melt-rock reaction.

This process would have caused olivine consumption and formation of new pyroxenes ± spinel ± garnet ± plagioclase via refertilization processes. However, the post-kinematic refertilization hypothesis is not consistent with the fact that these lherzolites register the lowest equilibrium T (Fernández-Roig and Galán, 2015), unless this process would have been pre-kinematic with respect to the development of the A- and D-type fabrics.

Deformation of the lithospheric mantle in NE Spain

Olivine CPO in the studied mantle rocks could be the result of the last significant tectonic event, of the present asthenosphere dynamic flow, or of a combination of both factors (Savage, 1999; Vauchez et al., 2012). On the one hand, the SCLM is usually deformed coherently with its crust, especially by strike slip faults of lithospheric scale and in transform plate boundaries (Vauchez et al., 2012). On the other hand, the Hercynian orogenesis is the most significant in the area and is characterized by late W-E to NW-SE oriented strike-slip faults, compatible with transpressional deformation, in the nearby Pyrenees (Carreras and Capella, 1998; Carreras, 2001). Therefore, we suggest that these Hercynian faults would have affected not only the crystalline crustal basement but also the underlying SCLM leading to the development of the olivine [010]-fiber (AG-type) fabric. Subsequent annealing would have preserved this fabric unchanged. The annealing and grain growth observed in protogranular peridotites would have been most likely aided by asthenospheric upwelling and percolation of mantle-derived magmas during Late Hercynian decompression, Permian and Cretaceous rifting episodes. Accordingly, the alkaline-carbonatite cryptic metasomatism registered by all harzburgites and some lherzolites was related to the Cretaceous lamprophyres (Galán et al., 2008; Galán and Oliveras, 2014). Late to post-Hercynian refertilization of the SCLM may have also occurred, but no clear relationships with olivine CPO were observed. The Alpine orogenesis was less intense in the Catalan Costal Ranges than in the Pyrenees, but late Alpine extensional faults did cause the formation of Neogene basins during or post-dating the ECRIS formation. SCLM

exhumation during Neogene-Quaternary periods may have taken place through extensional shear zones developed at lower T and P (Vauchez et al., 2012). These mantle extensional shear zones could be related to NW-SE Neogene normal faults, such as the Llorà fault (Fig. 1B) with a transtensional component. This fault may extend down to the lower crust and shallower lithospheric mantle since the presence of mantle and lower-crust xenoliths is restricted to the volcanoes related to this structure (Bolós et al., 2014). The significant change in the deformation regime, from dominant transpressive to mainly transtensive, would have transformed the earlier olivine [010]-fiber fabric (Vauchez et al., 2000) into orthorhombic (A-type) and [100]-fiber (D-type) fabrics mainly through SR and GBM dynamic recrystallization.

Conclusions

All spinel lherzolites, harzburgites and olivine websterites found as mantle xenoliths in Neogene-Quaternary alkaline basaltic lavas from the Catalan Volcanic Zone show protogranular microstructure, but among lherzolites there are also subordinate porphyroclastic and equigranular microstructures with gradual transition between the three types.

Harzburgites, the websterite and most lherzolites with protogranular microstructure have olivine [010]-fiber deformation fabric. The remaining lherzolites, mostly porphyroclastic and equigranular, show orthorhombic and rarely [100]-fiber deformation fabrics. The three types share the same [100]-glide direction. However, activation of dislocations slippping in [001] is also deduced from olivine misorientations.

The fabric strength of olivine decreases from protogranular harzburgites, clinopyroxene-poor lherzolites and the sole websterite towards finer-grained porphyroclastic and equigranular lherzolites.

The [010]-fiber fabric is associated with deformation by simple shear or transpression, probably related to late-Hercynian strike-slip shear zones. Subsequent annealing and grain growth would have preserved this fabric. The injection of mantle-derived magmas

during late Hercynian decompression, Permian and Cretaceous rifting episodes would have favoured these processes. Later on, the dominant [010]-fiber fabric would have been reactivated and transformed into orthorhombic and [100]-fiber types through SR and GBM dynamic recrystallization. These changes took place at higher stress and lower T and P and were due to changes in the deformation regime, from transpression or simple shear to mainly transtension. Late Alpine extensional movements leading to the formation of the European Cenozoic rift would cause the transtensional deformation.

Acknowledgments

References

Amelinckx, S. and Dekeyser, W. (1959): The structure and properties of grain boundaries. *Solid State Physics*, 8: 325-499.

Ancochea, E. (2004): El vulcanismo neógeno peninsular. In: Vera J. A. (ed.): *Geología De España.* Sociedad Geológica de España-Instituto Geológico y Minero de España, Madrid, 671-672.

Bascou, J., Delpech, G., Vauchez, A., Moine, B. N., Cottin, J. Y. and Barruol, G. (2008): An integrated study of microstructural, geochemical, and seismic properties of the lithospheric mantle above the Kerguelen Plume (Indian Ocean). *Geochemistry Geophysical Geosystems,* 9: Q04036. http:// dx.doi.org:10.1029/2007GC001879.

Bascou, J., Doucet, L. S., Saumet, S., Ionov, D. A., Ashchepkov, I. V. and Golovin, A. V. (2011): Seismic velocities, anisotropy and deformation in Siberian Cratonic Mantle: EBSD data on xenoliths from the Udachnaya Kimberlite. *Earth and Planetary Sciences Letters,* 304: 71-84.

Ben Ismaïl, W. and Mainprice, D. (1998): An olivine fabric database: an overview of upper mantle fabrics and seismic anisotropy. *Tectonophysics,* 296: 145-157.

Ben Ismaïl, W., Barruol, G., and Mainprice, D. (2001): The Kaapvaal Craton seismic anisotropy: petrophysical analyses of upper mantle kimberlite nodules. *Geophysical Research Letters,* 28: 2497-2500.

Bianchini, G., Beccaluva, L., Bonadiman, C., Nowell, G., Pearson, G., Siena, F. and Wilson, M. (2007): Evidence of diverse depletion and metasomatic events in harzburgite–lherzolite mantle xenoliths from the Iberian Plate (Olot, NE Spain): implications for lithosphere accretionary processes. *Lithos,* 94: 25-45.

Bodinier, J. L., Garrido, C. J., Chanefo, I., Bruguier, O. and Gervilla, F. (2008): Origin of pyroxenite– peridotite veined mantle by refertilization reactions: evidence from the Ronda Peridotite (Southern Spain). *Journal of Petrology,* 49: 999-1025.

Bolós, X., Martí, J., Becerril, L., Planagumà, Ll., Grosse, P. and Barde-Cabusson, S. (2014): Volcano structural-analysis of La Garrotxa volcanic Field (NE Iberia): Implications for the plumbing system. *Tectonophysics,* 642: 58-70.

Brey, G. P. And Köhler, T. P. (1990): Geothermobaromety in four-phase lherzolites II. New thermobarometers, and practical assessment of existing thermobarometers. *Journal of Petrology,* 31:1353-1378.

Bunge, H. J. (1982): *Texture analysis in materials sciences.* Buttleworth, London, 593 p.

Carreras, J. (2001): Zooming on northern Cap de Creus shear zones. *Journal of Structural Geology,* 23: 1457-1486.

Carreras, J. and Capella, I. (1994): Tectonic levels in the palaeozoic basement of the Pyrenees: a review and a new interpretation. *Journal of Structural Geology,* 16: 1509-1524.

CARTER, N. L. AND AVÉ LALLEMANT, H. G. (1970): High temperature flow of dunite and peridotite. *Geological Society of America Bulletin*, 81: 2181-2202.

COUVY, H. FROST, D. J., HEIDELBACH, F. NYILAS, K. UNGÁR, T. MACKWELL, S. AND CORDIER, P. (2004): Shear deformation experiments of forsterite at 11 Gpa–1400 °C in the multianvil apparatus. *European Journal of Mineralogy*, 16: 877-889.

DE KLOE, R. (2001): *Deformation mechanisms and melt nano-structures in experimentally deformed olivine–orthopyroxene rocks with low melt fractions. An electron microscopy study*. Ph.D. Thesis, Utrecht University, 173 p.

DIJKSTRA, A. H., BARTH, M. G., DRURY, M. R., MASON, P. R. D. AND VISSERS, R. L. M. (2003): Diffuse porous melt flow and melt–rock reaction in the lithospheric mantle at a slow-spreading ridge: a structural petrology and LA-ICP-MS study of the Othris Peridotite Massif (Greece). *Geochemistry Geophysics Geosystems*, 4: 8613. http://dx.doi.org/10.1029/2001GC000278.

ENRIQUE, P. (2009): Las espesartitas, camptonitas y bostonitas del complejo intrusivo de Aiguablava (Cadenas Costeras Catalanas): cartografía y composición. *Geogaceta,* 47: 125-128.

ESTEVE, S., ENRIQUE, P. AND GALÁN, G. (2014): The camptonites in the multiple intrusion of Platja Fonda (Girona, NE Spain): mechanisms of intrusion and geochemistry. *Journal of Geosciences*, 59: 23-40.

FALUS, G., TOMMASI, A. AND SOUSTELLE, V. (2011): Effect of dynamic recrystallization on olivine crystal preferred orientations in mantle xenoliths deformed under varied stress conditions. *Journal of Structural Geology*, 33: 1528-1540.

FERNÁNDEZ-ROIG, M. AND GALÁN, G. (2015): Microestructuras y química mineral de lherzolitas en xenolitos mantélicos de Cataluña (NE España). *Geogaceta*, 57: 3- 6.

FERNÁNDEZ-ROIG, M. GALÁN, G. AND MARIANI, E. (2015*a*): Microstructures and crystallographic preferred orientations in the subcontinental lithospheric mantle of NE Spain: EBSD data on xenoliths from the Catalan Volcanic Zone. *Microstructural evolution during HT deformation: advances in the characterization techniques and consequences to physical propertie*s. MicroDICE. 1 p.

FERNÁNDEZ-ROIG, M. GALÁN, G. AND MARIANI, E. (2015b): Crystal-preferred orientations of minerals from mantle xenoliths in alkali basaltic rocks form the Catalan Volcanic Zone (NE Spain). *Geophysical Research Abstracts*, 17: EGU2015-11482.

FRANK, F. C. (1950): *Report on the Conference on Plastic Deformation of Crystalline Solids*. Carnegie Institute of Technology and Office of Naval Research, Washington, 150 p.

GALÁN, G., OLIVERAS, V. AND PATERSON, B. A. (2008): Types of metasomatism in mantle xenoliths in Neogene–Quaternary alkaline mafic lavas from Catalonia (NE Spain). In: Coltorti, M. and Grégoire, M. (eds.): *Metasomatism in oceanic and continental lithospheric mantle*. Geological Society, London, Special Publication, 293: 121-153.

GALÁN, G. OLIVERAS, V. AND PATERSON, B. A. (2011): Thermal and redox state of the subcontinental lithospheric mantle of NE Spain from thermobarometric data on mantle xenoliths. *International Journal of Earth Sciences*, 100: 81-106.

GALÁN, G. AND OLIVERAS, V. (2014): Melting and metasomatism in the lithospheric mantle of NE Spain: Geochemical and Sr-Nd isotopic characteristics. *Chemical Geology*, 366: 75-89.

HARTE, B. (1977): Rock nomenclature with particular relation to deformation and recrystallisation textures in olivine-bearing xenoliths. *Journal of Petrology*, 85: 279-288.

HIDAS, K., FALUS, G., SZABÓ, C., SZABÓ, P. J., KOVÁCS, I. AND FÖLDES, T. (2007): Geodynamic implications of flattened tabular equigranular textured peridotites from the Bakony–Balaton Highland volcanic field (Western Hungary). *Journal of Geodynamics*, 43: 484-503.

HIGGIE, K. AND TOMMASI, A. (2014): Deformation in a partially molten mantle: constraints from plagioclase-lherzolites from Lanzo, Western Alps. *Tectonophysics,* 615-616: 167-181.

HOLTZMAN, B. K., KOHLSTEDT, D. L., ZIMMERMAN, M. E., HEIDELBACH, F., HIRAGA, T. AND HUSTOFT, J. (2003): Melt segregation and strain partitioning; implications for seismic anisotropy and mantle flow. *Science,* 301: 1227-1230.

HUMBERT, M. CEY, N. MULLIER, J. AND ESLING, C. (1996): Determination of mean orientation from a cloud of orientations. Application to electron backscatterring pattern measurements. *Journal of Applied Crystallography,* 29: 662-666.

JOHANESEN, K. E. AND PLATT, J. P. (2015): Rheology, microstructure, and fabric in a large scale mantle shear zone, Ronda Peridotite, Southern Spain. *Journal of Structural Geology*, 73: 1-17.

JUNG, H. AND KARATO, S. I. (2001): Water-induced fabric transitions in olivine. *Science,* 293: 1460-1464.

JUNG, H., KATAYAMA, I., JIANG, Z., HIRAGA, T. AND KARATO, S. (2006): Effect of water and stress on the lattice-preferred orientation of olivine. *Tectonophysics,* 421: 1-22.

JUNG, S., JUNG, H., AND AUSTRHEIM, H. (2014): Characterization of olivine fabrics and mylonite in the presence of fluid and implications for seismic anisotropy and shear localization. *Earth, Planets Space*, 66: 46.

KACZMAREK, M. A. AND MÜNTENER, O. (2008): Juxtaposition of melt impregnation and high-temperature shear zones in the upper mantle; field and petrological constraints from the Lanzo Peridotite (Northern Italy). *Journal of Petrology,* 49: 2187-2220.

KACZMAREK, M. A. AND TOMMASI, A. (2011): Anatomy of an extensional shear zone in the mantle (Lanzo Massif, Italy). *Geochemistry Geophysics Geosystems*, 12: Q0AG06. http://dx.doi.org/10.1029/2011gc003627.

KARATO, S.I., TORIUMU, M. AND FUJII, T. (1980): Dynamic recrystallization of olivine single crystals during high-temperature creep. *Geophysical Research Letters,* 7: 649-652.

KARATO, S.I., JUNG, H., KATAYAMA, I. AND SKEMER, P. (2008): Geodynamic significance of seismic anisotropy of the upper mantle: new insights from laboratory studies. *Annual Review of Earth and Planetary Sciences*, 36: 59-95.

KATAYAMA, I., JUNG, H. AND KARATO, S. I. (2004): New type of olivine fabric from deformation experiments at modest water content and low stress. *Geology*, 32: 1045-1048.

KATAYAMA, I. AND KARATO, S. (2006): Effects of temperature on the B- to C-type fabric transition in olivine. *Physical Earth and Planetary Interiors*, 157: 33-45.

KELEMEN, P. B. DICK, H. J. B. AND QUICK, J. E. (1992): Formation of harzburgite by pervasive melt/rock reaction in the upper mantle. *Nature*, 358: 635-41.

KÖHLER, T. P. AND BREY, G. P. (1990): Calcium exchange between olivine and clinopyroxene calibrated as a geothermobarometer for natural peridotites from 2 to 60 Kb with applications. *Geochemical and Cosmochimia Acta*, 54: 2375-2388

KOVÁCS, I., FALUS, G., STUART, G., HIDAS, K., SZABÓ, C., FLOWER, M. F. J., HEGEDUS, E., POSGAY, K. AND ZILAHI-SEBESS, L. (2012): Seismic anisotropy and deformation patterns in upper mantle xenoliths from the central Carpathian-Pannonian Region: asthenospheric flow as a driving force for Cenozoic extension and extrusion? *Tectonophysics,* 514-517: 168-179

LE ROUX, V. BODINIER, J. L., TOMMASI, A., ALARD, O., DAUTRIA, J. M., VAUCHEZ, A. AND RICHES, A. J. V. (2007): The Lherz spinel lherzolite: refertilized rather than pristine mantle. *Earth and Planetary Science Letters*, 259: 599–612.

LE ROUX, V., TOMMASI, A. AND VAUCHEZ, A. (2008). Feedback between deformation and melt percolation

in an exhumed lithosphere–asthenosphere boundary. *Earth and Planetary Science Letters*, 274: 401-413.

LEE, K., JIANG, Z. AND KARATO, S. (2002): A scanning electron microscope study of the effects of dynamic recrystallization on lattice preferred orientation in olivine. *Tectonophysics*, 351: 331-341.

LEWIS, C. J., VERGÉS, J. AND MARZO, M. (2000): High mountains in a zone of extended crust: insights into the Neogene-Quaternary topographic development of northeastern Iberia. *Tectonics,* 19: 86-102.

LLOYD, G. E., SCHMIDT, N. H., MAINPRICE, D. AND PRIOR, D. J. (1991): Crystallographic textures. *Mineralogical Magazine*, 55: 331-345.

LOSANTOS, M., MONTANER, J., SOLÀ, J., MATÓ, E., SAMPSÓ, J. M., PICART, J., CALVET, F., ENRIQUE, P., FERRÉS, M. Y. AND SOLÉ, J. (2000): *Mapa geològic de Catalunya 1:25.000, Palafrugell* 335- 1-1 (79-25). ICC (Servei Geològic de Catalunya).

MAINPRICE, D. (2007): Seismic anisotropy of the deep earth from a mineral and rock physics perspective In: Schubert, G. (ed.): *Treatise on Geophysics 2,* Elsevier, Oxford: 437-492.

MAINPRICE, D., TOMMASI, A., COUVY, H., CORDIER, P. AND FROST, D. J. (2005): Pressure sensitivity of olivine slip systems and seismic anisotropy of Earth's upper mantle. *Nature,* 433: 731-733.

MAINPRICE, D. BACHMANN, F. HIELSCHER, R. AND SCHAEBEN, H. (2015): Descriptive tools for the analysis of texture projects with large datasets using MTEX – strength, symmetry and components. In: *Rock deformation from field, experiments and theory. A volume in honour of Rutter.* Geological Society, London, Special Publication 409: 251-271.

MARTÍ, J. (2004): La región volcánica de Gerona. In: *Geología de España* (J.A. Vera, Ed.). Sociedad Geológica de España. Instituto Geológico y Minero de España, Madrid: 672-675.

MARTÍNEZ-POZA, A. I., DRUGUET, E., CASTAÑO, L. M. AND CARRERAS, J. (2014): Dyke intrusion into a pre-existing joint network: the Aiguablava lamprophyre dyke swarm (Catalan Coastal Ranges). *Tectonophysics,* 630: 75-90.

MERCIER, J. C. C. AND NICOLAS. A. (1975): Textures and fabrics of upper mantle peridotites as illustrated by xenoliths from basalts. *Journal of Petrology,* 16: 454-487.

PALASSE, L. N., VISSERS, R. L. M., PAULSSEN, H., BASU, A. R., AND DRURY, M. R. (2012): Microstructural and seismic properties of the upper mantle underneath a rifted continental terrane (Baja California): an example of sub-crustal mechanical asthenosphere? *Earth and Planettary Science Letter*s, 345-348: 60-71.

OHUCHI, T., KAWAZOE, T., NISHIHARA,Y., NISHIYAMA, N., IRIFUNE, T. (2011): High pressure and temperature fabric transitions in olivine and variations in upper mantle seismic anisotropy. Earth and Planetary Science Letters, 304, 55-63.

PASSCHIER, C. W. AND TROUW, R. A. J. (2005): *Microtectonics*. Springer-Verlag, Berlin/Heidelberg, 366 p.

PRIOR, D. J., MARIANI, E. AND WHEELER, J. (2009): EBDS in earth Sciences: Aplications, common practice, and challenges. In: Schwartz, A. J., Kumar, M., Adams B. L. and Field, D. P. (eds.): *Electron Backscatter Diffraction in Materials Science*. Springer: 345-360.

RAMPONE, E., VISSERS, R. L. M., POGGIO, M., SCAMBELLURI, M., AND ZANETTI, A. (2010): Melt migration and intrusion during exhumation of the Alboran lithosphere: the Tallante mantle xenolith record (Betic Cordillera, SE Spain). *Journal of Petrology,* 51, 295-325.

ROCA, E. AND DESEGAULX, P. (1992): Analysis of the geological evolution and vertical movements in the València Trough area, western Mediterranean. *Marine and Petroleum Geology,* 9: 167-176.

SAVAGE, M. K. (1999): Seismic anisotropy and mantle deformation: what have we learned from shear wave splitting? *Reviews of Geophysics,* 37: 65.106.

Solé Sabaris, L. (1962): Observaciones sobre la edad del volcanismo gerundense. *Memorias de la Real Academia de Ciencias y Artes de Barcelona,* 34: 359-372.

Solé, J., Pi, T. and Enrique, P. (2003) New geochronological data on the late Cretaceous alkaline magmatism of the northeast Iberian Peninsula. *Cretaceous Research*, 24: 135-140.

Soustelle, V., Tommasi, A., Bodinier, J. L., Garrido, C. J. and Vauchez, A. (2009): Deformation and reactive melt transport in the mantle lithosphere above a large-scale partial melting domain: the Ronda Peridotite Massif, Southern Spain. *Journal of Petrology*, 50: 1235-1266.

Soustelle, V. Tommasi, A. Demouchy, S. and Ionov, D. A. (2010): Deformation and fluid, a rock interaction in the supra-subduction mantle: microstructures and water contents in peridotite xenoliths from the Avacha Volcano, Kamchatka. *Journal of Petrology*, 51: 363-394.

Szabó, C. S., Falus, G. Y., Zajacz, Z., Kovács, I., and Bali, E. (2004): Composition and evolution of lithosphere beneath the Carpathian-Pannonian Region: a review. *Tectonophysics.* 393: 119-137.

Tommasi, A., Tikoff, B. and Vauchez, A. (1999): Upper mantle tectonics: three-dimensional deformation, olivine crystallographic fabrics and seismic properties. *Earth and Planetary Science Letters*, 168: 173-186.

Tommasi, A., Mainprice, D., Canova, G. and Chastel, Y. (2000): Viscoplastic self-consistent and equilibrium-based modeling of olivine lattice preferred orientations: implications for the upper mantle seismic anisotropy. *Journal of Geophysical Research, Solid Earth*, 105: 7893-7908.

Tommasi, A., Vauchez, A., Godard, M. and Belley, F. (2006): Deformation and melt transport in a highly depleted peridotite massif from the Canadian Cordillera: implications to seismic anisotropy above subduction zones. *Earth and Planetar Science Letters*, 252: 245-259.

Tommasi, A., Vauchez, A. and Ionov, D. (2008): Deformation, static recrystallization, and reactive melt transport in shallow subcontinental mantle xenoliths (Tok Cenozoic Volcanic Field, SE Siberia). *Earth and Planetary Science Letters,* 272: 65-77.

Tournon, J. (1968): *Le volcanisme de la province de Gérone (Espagne). Études de basaltes quaternaires et de leurs enclaves.* Thèse 3e Cycle, Université de Paris, 120 p.

Ubide, T., Lago, M., Arranz, E., Galé, C. And Larrea, P. (2010): The lamprophyric sub-vertical dyke swarm from Aiguablava (Catalonian Coastal Ranges): petrology and composition. *Geogaceta,* 49: 75-78.

Ubide, T., Arranz, E., Lago, M., Galé, C. and Larrea, P. (2012): The influence of crystal settling on the compositional zoning of a thin lamprophyre sill: a multi-method approach. *Lithos,* 132-133: 37-49.

Van Der Wal, D. Chopra, P. Drury, M. and Fitzgerald, J. (1993): Relationships between dynamically recrystallized grain size and deformation conditions in experimentally deformed olivine rocks. *Geophysical Research Letters*, 20: 1479-1482.

Vauchez, A. Tommasi, A. Barruol, G. and Maumus, J. (2000): Upper mantle deformation and seismic anisotropy in continental rifts. *Physics and Chemistry of the Earth*, 25: 111-117.

Vauchez, A. and Garrido, C. (2001): Seismic properties of an asthenospherized lithospheric mantle: constraints from lattice preferred orientations in peridotite from the Ronda Massif. *Earth and Planetary Science Letters*, 192: 235-249.

Vauchez, A., Dineur, F. and Rudnick, R. L. (2005): Microstructure, texture and seismic anisotropy of the lithospheric mantle above a mantle plume. Insights from the Labait Volcano xenoliths (Tanzania). *Earth and Planetary Science Letters*, 232: 295-314.

Vauchez, A., Tommasi, A. and Mainprice, D. (2012): Faults (shear zones) in the Earth's Mantle. *Tectonophysics*, 558-559: 1-27

Vollmer, F. W., 1990. An application of eigenvalue methods to structural domain analysis. *Geological Society of America Bulletin*, 102: 786-791.

Vonlanthen, P., Kunze, K., Burlini, L. and Grobety, B. (2006): Seismic properties of the upper mantle beneath Lanzarote (Canary Islands): model predictions based on texture measurements by EBSD. *Tectonophysics*, 428: 65-85.

Woodcock, N. H. and Naylor, M. A. (1983): Randomness testing in three-dimensional orientation data. *Journal of structural geology*, 5: 539-548.

Zaffarana, C., Tommasi, A., Vauchez, A. and Grégoire, M. (2014): Microstructures and seismic properties of south Patagonian mantle xenoliths (Gobernador Gregores And Pali Aike). *Tectonophysics,* 621: 175-197.